

Blowing in the wind

I. Velocities of chondrule-sized particles in a turbulent protoplanetary nebula

Jeffrey N. Cuzzi^{a,*} and Robert C. Hogan^b

^a *Space Science Division, NASA Ames Research Center, Moffett Field, CA 94035, USA*

^b *Bay Area Environmental Research, Inc. Sonoma, CA 95476, USA*

Received 26 September 2002; revised 23 January 2003

Abstract

Small but macroscopic particles—chondrules, higher temperature mineral inclusions, metal grains, and their like—dominate the fabric of primitive meteorites. The properties of these constituents, and their relationship to the fine dust grains which surround them, suggest that they led an extended existence in a gaseous protoplanetary nebula prior to their incorporation into their parent primitive bodies. In this paper we explore in some detail the velocities acquired by such particles in a turbulent nebula. We treat velocities in inertial space (relevant to diffusion), velocities relative to the gas and entrained microscopic dust (relevant to accretion of dust rims), and velocities relative to each other (relevant to collisions). We extend previous work by presenting explicit, closed-form solutions for the magnitude and size dependence of these velocities in this important particle size regime, and we compare these expressions with new numerical calculations. The magnitude and size dependence of these velocities have immediate applications to chondrule and CAI rimming by fine dust and to their diffusion in the nebula, which we explore separately.

© 2003 Elsevier Inc. All rights reserved.

1. Background

1.1. Introduction

The fabric of the most primitive meteorites undoubtedly contains many clues as to their origin. While most chondrites are samples of surfaces that have been well worked over by impacts and stirring (“regolith breccias”), the dominance of chondrules and like-sized objects remains clear. How it came about that most chondrite parent bodies are so dominated by particles with such a well-defined range of physical, chemical, and petrographic properties remains one of the big puzzles of meteoritics. Since there are relatively few examples of anything larger than 0.1- to 10-mm size particles in most primitive planetesimals, the way such particles interact with the gaseous nebula is of prime importance.

Fe–Mg–Si–O mineral chondrules, which solidified from a melt, constitute 30–80% of primitive meteorites. There are a number of extant hypotheses for the formation of the chon-

drules. Most workers in the field believe that chondrules are formed by either localized or nebula scale energetic events operating on freely floating precursors of comparable mass, at some location or locations in the protoplanetary nebula. However, some still maintain they are made in or on primitive bodies, or in collisions between them. In a hybrid scenario, some suggest they are formed in shock waves generated by already-formed planetesimals and thus that they are a secondary phenomenon to primary accretion of planetesimals. See, e.g., Grossman (1989), Grossman et al. (1989), Boss (1996), Connolly and Love (1998), and Jones et al. (2000) for reviews of hypotheses on this long-controversial and perennially fascinating subject.

Another meteorite constituent of great interest is the mineral grains called Ca–Al-rich refractory inclusions (CAIs)—so-called because their constituent minerals condense out of nebula gas at a much higher temperature than do chondrules. These objects are widely believed to be direct nebula condensates and have a complex subsequent thermal history which has some similarities to that of chondrules and some differences. There is some indication from radioisotope ages that CAIs might be $\sim 10^6$ years older than the chondrules,

* Corresponding author.

E-mail address: cuzzi@cosmic.arc.nasa.gov (J.N. Cuzzi).

but this remains slightly controversial. They make up 1–10% of primitive meteorites depending on type, and their size distribution is broader than that of the chondrules. How these high-temperature minerals find themselves intimately mixed with lower temperature minerals remains a puzzle.

It remains unresolved at this time whether the nebula gas was turbulent or laminar during the chondrule era. In previous papers, we have suggested that some of the observed properties of chondrules themselves—their typical size and size distribution—can be associated with, and easily explained by, the effects of weak nebula turbulence (Cuzzi et al., 1996, 2001). Nevertheless, a consistent end-to-end scenario for *formation* of primitive bodies in this environment, which relies on these processes, is not yet in hand. In this paper, we focus on the velocity evolution of this specific class of particles in a weakly turbulent nebula as a step toward developing a more complete scenario that operates to produce primitive bodies in a similar way across a variety of environments. The velocity evolution is critical for our understanding of several important aspects of chondrules and chondrites:

- (a) the radial distribution and redistribution or transport of chondrules and/or CAIs, once formed, before their accumulation into parent bodies;
- (b) the presence of fine-grained rims on chondrules, CAIs, and other coarse particles in primitive chondrites (Metzler and Bischoff, 1996; Brearley and Jones, 1998); and
- (c) collision rates and velocities between chondrule-sized particles.

The main goal of this paper is to provide a theoretical framework within which we can better understand millimeter- to centimeter-size particle evolution in general. We accomplish this in Sections 2 (new gas velocity autocorrelation function and analytical approximations) and 3 (new supporting numerical calculations). In other papers we apply these results to diffusion and dust rimming of meteorite constituents (Cuzzi et al., 2003; Cuzzi, in preparation).

1.2. Particle velocities in turbulence

Astrophysical modeling of the basic physics of particle behavior in fluid flows, whether laminar or turbulent, tends to begin and end with the classic papers by Whipple (1973), Adachi et al. (1976), Weidenschilling (1977, 1980), and Völk et al. (1980, henceforth VJMR; also Völk et al., 1978), with important recent updates by Markiewicz et al. (1991; henceforth MMV). In the fluid dynamics literature, however, the study of particle motions in fluid flows has both a long history and a robust ongoing presence. This history is nicely summarized by Meek and Jones (1973). More recent work in the fluids literature is noted in various relevant places in the following. VJMR first developed a useful formalism for calculating the dispersion velocities V_p (relative to inertial space) and collision velocities V_{pp} (relative

to each other) of particles in a turbulent nebula. They circumvented the thorny problem of “essential nonlinearity” (cf. Meek and Jones, 1973) by translating clever physical insights into mathematics and adopting a velocity autocorrelation function approach, which we discuss in more detail later. While the relative velocity between particles and gas, V_{pg} , serves an important internal role in their solutions, neither VJMR nor MMV say much about it. Yet, V_{pg} is the determinant quantity for accretion of rims of fine dust grains by small, macroscopic objects (Paque and Cuzzi, 1997; Cuzzi et al., 1998; Morfill et al., 1998). Our goal in this paper is to quantify V_p , V_{pg} , and V_{pp} for such particles in a way that expresses the formulation of VJMR and MMV in simple, analytical, closed-form solutions—allowing deeper insights to be gained into the history of chondrules and like-sized particles in the protoplanetary nebula.

In this paper, we determine velocities of all three kinds— V_p , V_{pg} , and V_{pp} —with emphasis on particles having stopping times t_s much less than the large eddy time scale, and, more specifically, comparable to the overturn time t_η of the smaller eddies. Particles in this size regime have behavior more complex than tiny “dust” grains, which are essentially trapped to the gas flow on all scales. In particular, particles with $t_s = t_\eta$ are subject to “preferential concentration” by large factors in turbulence, and based on some of its apparent fingerprints in the meteorite record, we have suggested a link among this process, chondrules, and primary accretion. Specifically, we refer to the fact that the *typical size* and the *shape of the size distribution* of chondrules are readily explained by turbulent concentration (Cuzzi et al., 1996, 2001). In other papers (Cuzzi et al., 2003; Cuzzi, in preparation) we explore the possibility that turbulent diffusion due to V_p might help us understand the puzzling mix of CAIs and chondrules in the same meteorites and that the functional form of V_{pg} might reveal still another fingerprint of turbulent concentration.

Particles are aerodynamically classified by their Stokes number St , the ratio of their stopping time t_s to the overturn time of some characteristic eddy. We will make use of Stokes numbers defined relative to two different eddy overturn time scales: the Stokes number relative to the largest, or integral scale, eddy time t_L : $St_L = t_s/t_L$, and that defined relative to the smallest, or Kolmogorov scale, eddy time t_η : $St_\eta = t_s/t_\eta$. The overturn time of the largest scale eddy t_L is generally regarded as the local orbit period. Preferentially concentrated particles (chondrules, we believe) have $St_\eta = 1$ and $St_L \ll 1$. For these particles, which are smaller than the gas molecular mean free path, the stopping time $t_s = r\rho_s/c\rho_g$, where r is particle radius, ρ_s is particle material density, c is the nebula sound speed, and ρ_g is the nebula gas density (Weidenschilling, 1977). That is, t_s and thus both St_L and St_η are *linearly proportional to particle radius*. Table 1 summarizes these and other terms.

Table 1
List of commonly used symbols

Parameter	Definition
c	gas molecule thermal speed
$E(k)$	turbulent kinetic energy at wavenumber k
H	nebula vertical scale height
k	eddy wavenumber
k_L	wavenumber of largest scale eddy
k_η	wavenumber of Kolmogorov (smallest) scale eddy
L	integral or largest scale in turbulent energy spectrum
r	particle radius
R	gas velocity autocorrelation function
Re	flow Reynolds number
St_L	Stokes number relative to largest eddy
St_η	Stokes number relative to Kolmogorov scale eddy
t_s	stopping time of particle due to gas drag
t_k	overturn time of eddy with wavenumber k
t_L	overturn time of largest eddy
t_η	overturn time of Kolmogorov scale eddy
V_g	gas turbulent velocity (large eddy)
V_p	particle random velocity in inertial space
V_{pg}	relative velocity between particles and gas
V_{pp}	relative velocity between particles
α	nebula viscosity parameter; $Re = \alpha cH/\nu$
ϵ	dissipation of turbulent kinetic energy
η	Kolmogorov scale
ν	molecular kinematic viscosity
ν_T	turbulent kinematic viscosity
ω	eddy temporal frequency
ρ_g	gas mass density

1.3. Previous work

We briefly review and simplify the notation of VJMR and MMV. VJMR assumed a fully developed inertial range of turbulent kinetic energy E , extending from some largest, or integral, scale $l = L$ to zero for the smallest scale. MMV also adopted the Kolmogorov energy spectrum (as shall we) but correctly pointed out that turbulence ceases for scales smaller than the Kolmogorov or inner scale $l = \eta$. Especially for small particles in the chondrule- and CAI-size range, MMV point out that this has important implications for V_p and V_{pp} ; we will show here that the implications are important for V_{pg} as well. Following VJMR, we work in the spatial frequency regime, where $k(l) = 1/l^1$ and $E(k) = E_L(k/k_L)^{-5/3}$ for the Kolmogorov spectrum. [Note that our $E(k)$ is a true energy and is half of VJMR's $P(k)$.] Then the velocity characterizing wavenumber k is $v(k) = (2kE(k))^{1/2}$ and the eddy time scale for wavenumber k (the energy exchange time scale of VJMR Eq. (17)) is $t(k) = 1/(kv(k)) = t_L(k/k_L)^{-2/3}$. As did MMV, we assume $E(k) = 0$ for $k > k_\eta$ (no turbulent energy at scales smaller than the Kolmogorov scale). The mean square turbulent (fluctuating) gas velocity is V_g^2 ; thus the typical turbulent kinetic energy per unit gas mass is $V_g^2/2$, providing the nor-

malization criterion

$$\int_{k_L}^{k_\eta} E(k) dk = V_g^2/2 = \int_{k_L}^{k_\eta} E_L(k/k_L)^{-5/3} dk = \frac{3}{2} E_L k_L. \quad (1)$$

These definitions lead to our specific definition of $t_L \equiv 1/k_L V_g$. The turbulent gas motions induce fluctuating velocities in the particle population, leading to diffusion (V_p), mutual collisions (V_{pp}), and motion relative to the local gas (V_{pg}).

VJMR derive V_p formally by a backward time integration of the instantaneous acceleration (their Eqs. (5) and (6)),

$$V_p(t) = t_s^{-1} \int_0^t \exp(-(t-t')/t_s) V_g(t') dt', \quad (2)$$

where $V_g(t')$ represents the fluctuating gas velocity history along a particle trajectory (formally unknown at this point). They proceed by approximating $V_g(t')$ as an integral over all (independently acting) spatial frequencies k with eddy time scales t_k , and approximate the contributions as coming from two classes of eddies: “class 1” eddies, with overturn times long enough ($t_k > t_s$) that particles are always in equilibrium within them and are primarily just advected by their (temporally fluctuating) motions, and “class 3” eddies with overturn times too short ($t_k < t_s$) for the particle to come to equilibrium as it passes through them. Intermediate, or what might be “class 2,” eddies are not treated separately but are simply absorbed into the classes on either side. Different simplifications are allowed for each class. The boundary between eddy classes 1 and 3 is k^* , where $t_{k^*} = t_s$. VJMR show that the class 3 (small, fast) eddies are negligible for velocity components V_p and V_{pg} but dominate the contributions to V_{pp} . We will make use of these results in the following.

VJMR first obtain the product $\langle V_p(t) V_p(t) \rangle = \langle V_p^2 \rangle$ by integrating backward over two separate time histories. They introduce the gas velocity autocorrelation function (ACF) for gas velocities in their Eq. (16): $R(t, t'; k) = (E(k)/2\pi k^2) \exp(-|t-t'|/t_k)$. While they do not emphasize the distinction, the ACF to be used in this way is properly Lagrangian, i.e., that determined *along a particle trajectory* (Batchelor, 1948; Hinze, 1975; Squires and Eaton, 1990; Elghobashi, 1991), which is a function of t_s in general. However, for $St_L \ll 1$, and at this stage of our knowledge, this dependence is weak and the distinction is not significant (cf. Squires, 1990; Squires and Eaton, 1991).

Subsequently, MMV suggested the more general, even if *ad hoc*, functional form

$$R(t, t'; k) = \frac{E(k)}{2\pi k^2} \left(1 + \frac{|t-t'|}{t_k} \right)^n e^{-|t-t'|/t_k}, \quad (3)$$

with $n = 0$ or 1. As with VJMR, the lack of t_s dependence makes this an Eulerian ACF. They note that the $n = 1$ case has more plausible physical behavior (zero slope) near $t = t'$ than the $n = 0$ (pure exponential) form assumed by VJMR.

The zero-slope behavior of $R(t, t'; k)$ arises because the time scales and spatial scales of realistic turbulence do not extend to zero, but have lower limits (the Kolmogorov time and length scales). In the next section, we present new results of two different kinds which validate the preference for $n = 1$.

2. New results

2.1. The form of the autocorrelation function and the value of n

The selection of $n = (0, 1)$ determines the form of the gas velocity autocorrelation function $R(t, t'; k)$. Squires (1990) and Squires and Eaton (1991) measured this function directly in direct numerical simulations of turbulence, by following gas motions along the trajectories of a number of particles with different St_L . We have now done the same, using our own three-dimensional (3D) numerical simulations (described in Hogan et al., 1999). The MMV ACF $R(t, t', k)$ (Eq. (3)) must be integrated over all 3D k -space to obtain the (normalized) temporal form

$$R(t, t') = \frac{1}{V_g^2} \int_0^{\infty} R(t, t', k) 4\pi k^2 dk.$$

For a general turbulent energy spectrum the energy-and-velocity-bearing length scale $L \equiv 1/k_L$ must be calculated as a weighted mean (e.g., Vincent and Meneguzzi, 1991) using

$$\begin{aligned} L &\equiv \frac{1}{k_L} = \int_0^{\infty} \frac{E(k)}{k} dk \bigg/ \int_0^{\infty} E(k) dk \\ &= \frac{2}{V_g^2} \int_0^{\infty} \frac{E(k)}{k} dk. \end{aligned}$$

For an inertial range, k_L is merely the smallest k (i.e., k_0 of VJMR), but for our noninertial range spectrum, the actual numerical result must be used. In Fig. 1 we compare the MMV velocity autocorrelation function for $n = 0$ and 1 with ACFs derived from numerical simulations described by Squires (1990) and Hogan et al. (1999). The simulation ACFs, being along actual particle trajectories, are Lagrangian, and as mentioned in Section 1.3, the MMV ACFs are Eulerian. The small differences seen in the knee of the curve are consistent with the difference between Lagrangian and Eulerian ACFs, as observed in simulations (Squires, 1990; Squires and Eaton, 1991) and as predicted by theory (Nakao, 1997): The Lagrangian is always less than the Eulerian, even for a fluid.

The $n = 1$ model is clearly a better fit to the simulation results, even without making allowances for these possible deviations. While the pure exponential case (dashed line)

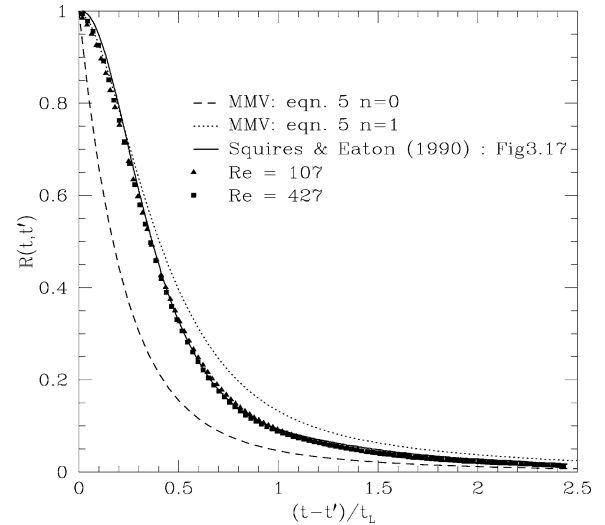


Fig. 1. Autocorrelation function for gas velocities along the trajectory of a $St_\eta = 1$ particle, as computed directly from our simulations (symbols, for $Re = 107$ and 427) and from the simulations of Squires (1990; solid line), compared with alternate theoretical approximations using the $n = 0$ (dashed) and $n = 1$ (dotted) models of MMV. The $n = 1$ model is the better choice because it displays *both* the zero slope at zero delay and the same width as the observed autocorrelation function (discussed in Section 2.1).

could be stretched horizontally by applying some arbitrary scale factor to the eddy time t_L , this would be physically unjustified and moreover would fail to reproduce the zero-slope behavior at zero time delay. This has important implications, primarily for V_{pg} and V_{pp} . In Section 3, we again use our own 3D numerical calculations to directly compare V_p and V_{pg} with the predictions of the two alternate autocorrelation functions, and we again reach the same conclusion.

2.2. Closed-form solutions for particle velocities in Kolmogorov turbulence

2.2.1. V_p : Particle random velocities relative to inertial space

After some algebra, VJMR derive an expression (their Eq. (18)) for the mean-square particle fluctuating velocity V_p , of which we need only the large, slow (class 1) eddy contribution since the small eddy contribution is negligible for $St_\eta = 1$ particles (we will henceforth drop the $\langle \rangle$ notation on V_p , V_g , V_{pg} , and V_{pp} and will merely recall that all are statistical expectation values based on extensive temporal or spatial averaging). Because of our emphasis on particles with $St_\eta = 1$, we also replace the upper limit of VJMR's class 1 integral (k^*) with the Kolmogorov scale k_η . This simplification is, in fact, actually fairly good over the entire range of $St_L \ll 1$, *precisely because* the contribution of eddies on scales smaller than k^* (the class 3 eddies) is negligible. That is, the upper limit can be extended from k^* to k_η *in general* for mathematical simplicity without incurring significant error. Mathematically, the upper limit could even be extended to infinity (e.g., Völk et al., 1980), but the important role of the Reynolds number and of the Kolmogorov scale is then

lost. Thus,

$$V_p^2 \approx 2 \int_{k_L}^{k_\eta} E(k) \frac{t_k}{t_k + t_s} dk. \quad (4)$$

Similarly, the basic equation (18) for V_p^2 of VJMR, generalized by MMV (their Eq. (6)) can be simplified to

$$\begin{aligned} V_p^2 &\approx 2 \int_{k_L}^{k_\eta} E(k) \left(1 - \left(\frac{t_s}{t_k + t_s}\right)^{n+1}\right) dk \\ &= 2 \int_{k_L}^{k_\eta} E(k) \left(1 - \left(\frac{1}{1 + t_k/t_s}\right)^{n+1}\right) dk \end{aligned} \quad (5)$$

for the particle size regime of interest here. As did VJMR, MMV note that the second integral of their Eq. (6)—the class 3 eddy contribution—is negligible for small particles, so Eq. (5) here retains only the first integral of their Eq. (6). We have again simplified the upper limit of integration in the remaining integral for the nominal $St_\eta \approx 1$ case, using $k^* \approx k_\eta \gg k_L$. We validate this by comparing our results with those of MMV (Section 2.3).

The result for V_p^2 was plotted, but not stated explicitly, by VJMR and MMV (Fig. 1 in both papers) and explicitly derived by Cuzzi et al. (1993, effectively for $n = 0$; Appendix B): $V_p^2 = V_g^2/(1 + St_L)$. It is simple to see why $V_p^2 \approx V_g^2$ in the limit $St_L \ll 1$ (and certainly for $St_\eta \approx 1$, where $St_L \approx Re^{-1/2}$) since $t_s \ll t_k$ in Eqs. (4) and (5) for nearly all k and overwhelmingly all $E(k)$. This limit is appropriate for chondrule- and CAI-sized particles even in the presence of their small vertical settling velocity—they diffuse nearly as well as a gas molecule and do not “settle to the midplane” in even a very weakly turbulent nebula (Dubrulle et al., 1995; Cuzzi et al., 1996). However, even for small particles, V_p^2 and V_g^2 are not *exactly* equal, resulting in a small, but very important, relative energy of motion V_{pg}^2 , giving the velocity with which particles move through the gas and encounter tiny (micrometer-sized) dust grains. We discuss this quantity next.

2.2.2. V_{pg} : Particle velocities relative to the gas

The average relative velocity magnitude between a particle and the turbulent gas is V_{pg} . VJMR make use only of the spatial frequency components of this quantity, which they refer to as $V_{rel}(k)$ (their Eq. (15)). Practically speaking, however, a particle will instantaneously sense all eddy contributions as one V_{pg} ; we obtain this by merely integrating VJMR Eq. (15) over k . If we consider only the part of the expression relevant for $St_\eta \approx 1$ (that for $k^* > k_L$), neglect any systematic velocity, and again let $k^* \approx k_\eta \gg k_L$, the second integral vanishes and we obtain

$$V_{pg}^2 \approx 2 \int_{k_L}^{k_\eta} E(k) \left(\frac{t_s}{t_k + t_s}\right) dk. \quad (6)$$

For this $n = 0$ case treated by VJMR, it can be easily verified using Eqs. (4) and (6) that

$$V_{pg}^2 + V_p^2 = 2 \int_{k_L}^{k_\eta} E(k) dk = V_g^2. \quad (7)$$

However, this useful result is true, independent of n . It may also be obtained by Fourier transform solution of the forcing equations in temporal frequency (ω) space, where the energy spectrum of gas velocity fluctuations $E_g(\omega)$, particle velocity fluctuations $E_p(\omega)$, and relative velocity fluctuations $E_{pg}(\omega)$ are related by

$$\begin{aligned} E_p(\omega) &= E_g(\omega)/(1 + t_s^2 \omega^2) \quad \text{and} \\ E_{pg}(\omega) &= t_s^2 \omega^2 E_p(\omega). \end{aligned} \quad (8)$$

This approach can be traced to Csanady (1963); it is also described by Hinze (1975, Chapter 5), Meek and Jones (1973), and Squires (1990, Sections 4.2 and 4.5.1). The E_p solution was also derived in this way by Cuzzi et al. (1993, Appendix B). It is also clear then that $E_{pg}(\omega) + E_p(\omega) = E_g(\omega)$, essentially the same result as Eq. (7) here. Finally, we have directly verified Eq. (7) in our numerical simulations.

Using this general relationship, we can extend the results of MMV to obtain V_{pg}^2 for their more generalized gas velocity autocorrelation functions (they only present results for V_p^2). That is, using Eqs. (1) and (5), we get

$$\begin{aligned} V_{pg}^2 &= V_g^2 - V_p^2 = 2 \int_{k_L}^{k_\eta} E(k) \left(\frac{t_s}{t_s + t_k}\right)^{n+1} dk \\ &= 2 \int_{k_L}^{k_\eta} E(k) \left(\frac{1}{1 + t_k/t_s}\right)^{n+1} dk. \end{aligned} \quad (9)$$

We will use Eqs. (5) and (9), with assumed inertial range expressions for $E(k)$, to derive analytical expressions for V_p and V_{pg} of hypothetically “chondrule-like” (i.e., $St_\eta \approx 1$) particles as functions of their size and the turbulent Reynolds number.

2.2.3. V_{pp} : Relative velocities between particles of similar sizes

Small particles of similar sizes are affected coherently by most eddies so move nearly coherently and can have very small *relative* velocities V_{pp} even if their inertial space velocities V_p are comparable to V_g . Expressions for V_{pp} (Völk et al., 1980, Appendix C and Eq. (19); Markiewicz et al., 1991, Eqs. (7) and (8)) are more cumbersome than for V_p or V_{pg} , but they respond nicely to certain simplifying assumptions. The full expression for V_{pp} for two particles of equal size is (changing notation slightly from MMV Eq. (9), and allowing for a finite Kolmogorov scale)

$$V_{pp}^2 = 4 \int_{k^*}^{k_\eta} E(k) \left(1 - \frac{t_s}{t_s + t_k}\right) \left[g(\chi) + \frac{nt_s h(\chi)}{t_s + t_k}\right] dk, \quad (10)$$

where $g(\chi) = \tan^{-1}(\chi)/\chi$ and $h(\chi) = 1/(1 + \chi^2)$. The parameter χ of VJMR and MMV is small in our regime of interest,

$$\chi = \frac{V_{\text{rel}}(k)t_s k t_k}{t_s + t_k} = \frac{V_{\text{rel}}(k)t_s}{v(k)(t_s + t_k)} \approx \frac{V_{\text{rel}}(k)}{2v(k)} < 1, \quad (11)$$

since in the very limited range of k over which the integral is done, $t_s \approx t_k$.² In fact $\chi \ll 1$ over most of the integral where $t_s \ll t_k$, so the functions $g(\chi)$ and $h(\chi)$ are ≈ 1 or perhaps as small as a fraction of order unity; thus

$$\begin{aligned} V_{\text{pp}}^2 &\approx 4 \int_{k^*}^{k_\eta} E(k) \left[1 - \left(\frac{t_s}{t_s + t_k} \right)^{n+1} \right] dk \\ &= 4 \int_{k^*}^{k_\eta} E(k) \left[1 - \left(\frac{1}{1 + t_k/t_s} \right)^{n+1} \right] dk. \end{aligned} \quad (12)$$

The integrand is identical to that for V_p^2 , but the integral has a different prefactor, as well as different limits, which make it clear that only the eddies faster than t_s can perturb identical particles into having incoherent relative velocities.

2.2.4. Inertial range (Kolmogorov) turbulence; scaling relations

The general Kolmogorov theory of fully developed turbulence provides a convenient and widely applicable mathematical representation of the turbulent energy spectrum. We follow VJMR and MMV in applying it, obtaining handy closed-form solutions for V_p , V_{pg} , and V_{pp} .

Recall that for the gas,

$$t_k = l(k)/v(k) = (L/V_g)(k/k_L)^{-2/3} = t_L(k/k_L)^{-2/3} \quad (13)$$

(Section 1.3; Cuzzi et al., 2001). In Eq. (13) we have made the usual identification of V_g with the largest scale eddy L . For the particles,

$$\frac{t_s}{t_L} = St_L = (k_s/k_L)^{-2/3} \quad (14)$$

and

$$\frac{t_s}{t_k} = (k/k_s)^{2/3} = \frac{t_s}{t_L} (k/k_L)^{2/3} = St_L (k/k_L)^{2/3}. \quad (15)$$

Note that if we restrict our attention to particles with $St_\eta = t_s/t_\eta \approx 1$, then their Stokes number referred to the *integral* scale automatically becomes

$$\begin{aligned} St_L = t_s/t_L = t_\eta/t_L &= (k_\eta/k_L)^{-2/3} = (Re^{3/4})^{-2/3} \\ &= Re^{-1/2}. \end{aligned} \quad (16)$$

The last substitution of $(k_\eta/k_L) = Re^{3/4}$, where $Re = LV_g/\nu$ is the flow Reynolds number, with ν being the molecular kinematic viscosity, is a direct consequence of the definitions of the Kolmogorov scale, the energy dissipation rate, and the Reynolds number (Tennekes and Lumley, 1972). This relation can be obtained without any reference at all to the Kolmogorov spectrum but by merely using scaling arguments relating to t_L and t_η .³ Re is related to astrophysical “ α ”-models of the protoplanetary nebula by $Re = \alpha cH/\nu$ with c = sound speed and H = nebula vertical scale height (Cuzzi et al., 2001).

2.2.5. Final expressions for V_{pg} and V_{pp} (and V_p)

Substituting the scaling relations in the previous section gives for Eq. (9)

$$\begin{aligned} V_{\text{pg}}^2 &= 2 \int_{k_L}^{k_\eta} E(k) \left(\frac{1}{1 + t_k/t_s} \right)^{n+1} dk \\ &= 2 \int_{k_L}^{k_\eta} E(k) \left(\frac{St_L}{St_L + (k/k_L)^{-2/3}} \right)^{n+1} dk. \end{aligned} \quad (17)$$

We use the normalization (Eq. (1)) to write

$$E(k) = \frac{V_g^2}{3k_L} \left(\frac{k}{k_L} \right)^{-5/3},$$

and we change integration variable to $x = k/k_L$, leaving

$$V_{\text{pg}}^2 = \frac{2V_g^2}{3} \int_1^{Re^{3/4}} \left(\frac{St_L}{St_L + x^{-2/3}} \right)^{n+1} x^{-5/3} dx, \quad (18)$$

where in the upper limit we have substituted $k_\eta/k_L = Re^{3/4}$ from the scaling relations. Closed-form solutions for Eq. (18) can be obtained for $n = 0$ or 1 . For example, for $n = 1$ the result of the integral is

$$\begin{aligned} V_{\text{pg}}^2 &= V_g^2 \left[\frac{St_L}{1 + St_L x^{2/3}} \right]_{Re^{3/4}}^1 \\ &= V_g^2 \left[\frac{St_L^2 (Re^{1/2} - 1)}{(St_L + 1)(St_L Re^{1/2} + 1)} \right]. \end{aligned} \quad (19)$$

For $n = 0$ the result of the integral is

$$V_{\text{pg}}^2 = V_g^2 \left[St_L \ln \left(\frac{Re^{1/2}(1 + St_L)}{Re^{1/2}St_L + 1} \right) \right]. \quad (20)$$

These results make it quite easy to predict both the magnitude and the St_η dependence of V_{pg} for arbitrary nebula turbulent intensity. We do not present V_p separately, because it is easily obtained using $V_p^2 = V_g^2 - V_{\text{pg}}^2$ (Eq. (9)).

² In the equation for χ , the mathematical generalization of V_{pg} by VJMR and MMV to its k th components $V_{\text{rel}}(k)$ momentarily reappears. However, it is true in general, at any spatial frequency, that the particle–gas relative velocity is less than, or at most equal to, the gas velocity itself.

³ Let the energy dissipation rate be ϵ . Then $\epsilon = V_g^2/t_L = V_g^3/L$, where t_L , the energy exchange time, is defined in Section 1.3. Also $t_\eta = (v/\epsilon)^{1/2}$ and $\eta = (v^3/\epsilon)^{1/4}$ (e.g., Tennekes and Lumley, 1972, Chapter 1). Solving gives $t_L/t_\eta = Re^{1/2}$ and $\eta/L = Re^{3/4}$.

We solve Eq. (12) for V_{pp} in a similar fashion to the solution for V_{pg} to obtain, for $n = 1$:

$$V_{pp}^2 = \frac{4V_g^2}{3} \int_{k(t_s)/k_L}^{k_\eta/k_L} \left(\frac{2St_L x^{-7/3} + x^{-9/3}}{St_L^2 + 2St_L x^{-2/3} + x^{-4/3}} \right) dx. \quad (21)$$

As before, the upper integration limit is $k_\eta/k_L = Re^{3/4}$. For the lower limit, $k^*/k_L = k(t_s)/k_L = (t_s/t_L)^{-3/2} = St_L^{-3/2}$ from the scaling relations. The closed-form analytic solution of this integral is:

$$\begin{aligned} V_{pp}^2 &= 2V_g^2 \left[\frac{x^{-2/3}}{1 + St_L x^{2/3}} \right]_{Re^{3/4}}^{St_L^{-3/2}} \\ &= 2V_g^2 \left[\frac{St_L}{2} - \frac{1}{St_L Re + Re^{1/2}} \right]. \end{aligned} \quad (22)$$

The $n = 0$ form of the solution is somewhat less useful, and we note it without expanding it as it will not be used further:

$$V_{pp}^2 = 2V_g^2 \left[St_L \ln \left(\frac{1 + St_L x^{2/3}}{x^{2/3}} \right) - \frac{1}{x^{2/3}} \right]_{St_L^{-3/2}}^{Re^{3/4}}. \quad (23)$$

2.3. Detailed comparisons with the models of Markiewicz et al.

2.3.1. Detailed MMV model

In addition to developing the analytical expressions discussed and applied in this paper, we also developed a detailed numerical model following the prescriptions of MMV exactly (but with a generalized turbulent energy spectrum). The full model is valid for all St_L . This was needed both to evaluate their theoretical approach in the context of our numerical simulations of turbulence (Section 3), which have a non-Kolmogorov spectrum and low Reynolds number compared to nebula applications, and to assess the validity of our analytical approximations. The numerical model of MMV is no longer in active use (W. Markiewicz, personal communication, 2002), so we digitized their V_{pp} results (their Fig. 5) to facilitate comparisons. As seen in Fig. 2, our full numerical model for V_{pp} (solid curves) agrees very well with their results for V_{pp} (long dashed curves). In Fig. 2 we also show our results for V_{pg} , not presented by VJMR or MMV, as obtained by integrating MMV Eq. (4) over all spatial frequencies. Note that we, and MMV, both use the appropriate form of $R(t, t'; k)$ (i.e., that for the correct choice of n ; Section 1.3) for these calculations.

The most striking feature of the results, first noted by MMV, is that V_{pp} very quickly falls to zero for similar sized particles with $St_\eta < 1$ (i.e., $St_L < Re^{-1/2}$, as shown in the scaling relations of Section 2.2.4) because there is no more energy in faster eddies to provide relative velocities to such particles. This does not happen to V_{pg} , because eddies on all scales contribute. Also note that V_p and V_{pp} decrease for large particles ($St_L > 1$), as fewer eddies can effectively couple to particles with such long stopping times. Naturally, V_{pg} simply approaches V_g for these large particles.

Upon comparing our original analytical results (Eqs. (19) and (22)) with our full numerical model and the MMV results, we found some small quantitative discrepancies at the order unity level, as might be expected. The responsible approximations were easily identified. First, we approximated the boundary between class 1 and class 3 eddies by $t_s = t(k^*)$, rather than the more complete Eq. (9) of VJMR and Eq. (4) of MMV, which gives the relevant eddy frequency in the moving frame of the particle and involves $V_{rel}(k)$. Comparison of the two criteria revealed that, to a very good approximation, the criterion $t_s = t(k^*)$ gives a value of k^* that is too large by a factor close to 2 (Fig. 3). So, after this ‘‘calibration,’’ we merely decrease the lower limit of integration in our Eq. (22) by a factor of 2. Second, even after this correction, our values of V_{pp} are about 20% high. This is easily ascribed to our approximation that $g(\chi)$ and $h(\chi)$ are equal to unity throughout the entire range of k ; in fact, they are tens of percent smaller than unity over some part of this range, depending on the value of St_L . Empirically, this is corrected by multiplying our analytical expression for V_{pp} by a constant factor of 0.8. With these two simple adjustments, each correcting a known oversimplification, our analytical expression for V_{pp} achieves very good agreement with the MMV results, and with our own full numerical model, over the relevant range of $St_L \lesssim 0.1$ or so. There appears to be no reason to make such refinements to our analytical expression for V_{pg} (Eq. (19)), because our approximations are better justified and the agreement with MMV acceptable.

Overall, the approximations succeed better than might be expected. While our assumptions are only demonstrably valid for $St_L \ll 1$, the results are demonstrably valid for $St_L \lesssim 0.1$.

2.3.2. Corrected equations based on comparison with MMV

With insights gained from comparison of our numerical and analytical models, we have made two small adjustments to Eq. (22) for V_{pp} which correct for two of our approximations. Equation (22) is multiplied by a factor of 0.8, and the upper integration limit ($St_L^{-3/2}$) is divided by 2, so the first term in the final expression changes from $St_L/2$ to $St_L/1.03 \approx St_L$. The approximations entering into our expression for V_{pg} are better, so no correction is applied. The final equation for V_{pp} is then

$$V_{pp}^2 = 1.6V_g^2 \left[St_L - \frac{1}{St_L Re + Re^{1/2}} \right]. \quad (24)$$

The results of Eqs. (19) and (24) (the preferred and adjusted $n = 1$ forms), normalized by V_g , are shown in Fig. 4 for the same three values of Re as in MMV and in close-up form in Fig. 5.

As shown by MMV (their Fig. 2), and as seen previously in our Fig. 2, the falloff of V_{pp} is extremely steep for $St_\eta < 1$ (i.e., $St_L < Re^{-1/2}$ as shown in the scaling relations of Section 2.2.4) because there is no more energy in faster eddies to provide relative velocities to such particles.

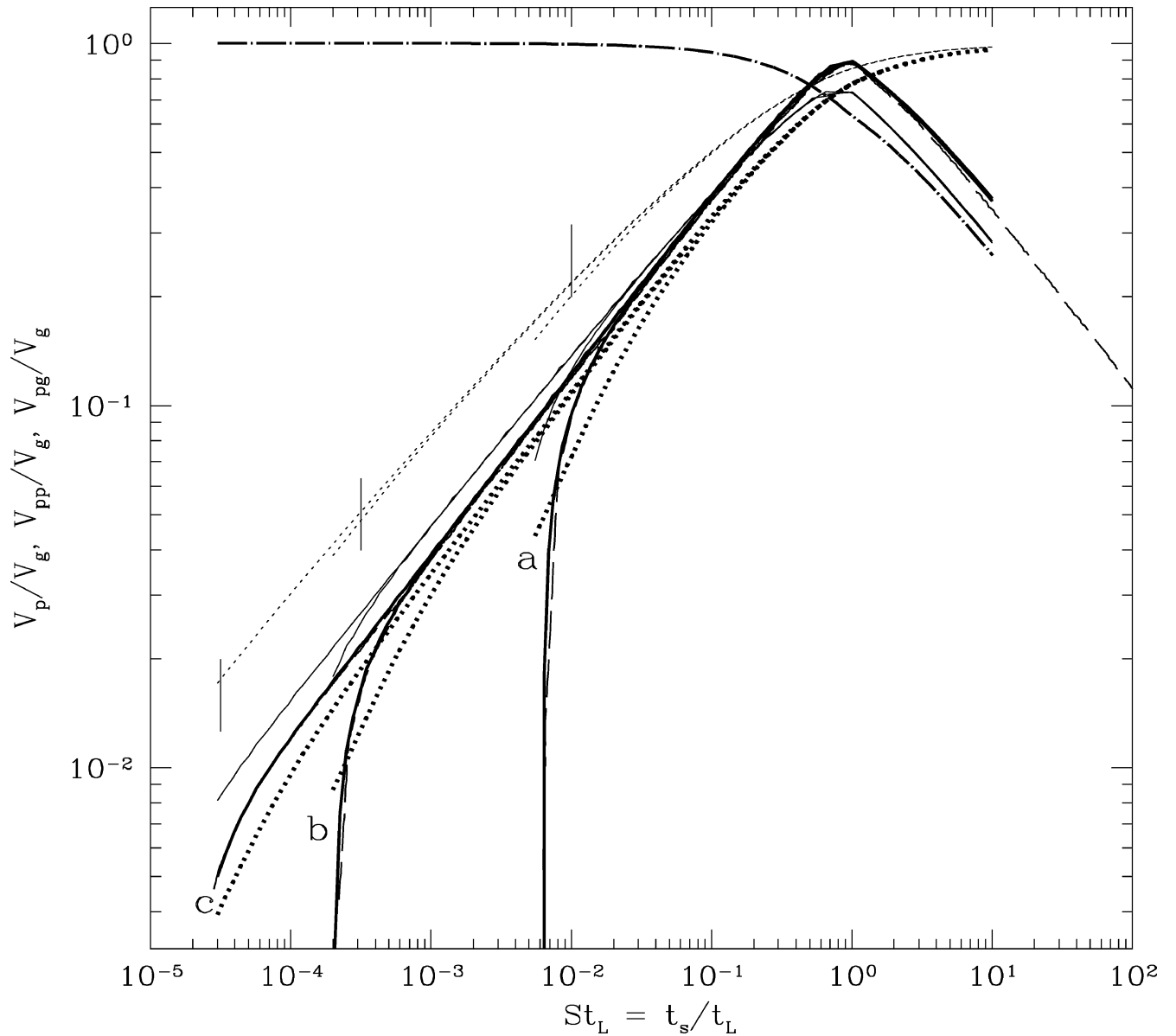


Fig. 2. Comparison of our numerical version of the full MMV models for $n = 0$ (light curves) and $n = 1$ (heavy curves) with digitized results for V_{pp} from MMV (dashed curves, their Fig. 5, for $n = 1$). Three different Re are shown: (a) 10^4 , (b) 10^7 , and (c) 10^9 . The dash-dot curves are for V_p ($n = 1$), which has the same shape for all three Re . V_{pg} is shown in the two sets of dotted curves and V_{pp} in the two sets of solid curves. Note that the $n = 0$ values of V_{pg} (light dotted curves) are considerably (3–4 times) higher than the preferred $n = 1$ values (heavy dotted curves), and the St_L dependence of V_{pg} , for $n = 0$, never gets much steeper than $St_L^{0.5}$, whereas for $n = 1$ a linear dependence is seen for $St_L < Re^{-1/2}$ ($St_\eta \lesssim 1$). As in Figs. 4 and 5, vertical tick marks indicate $St_L = Re^{-1/2}$ for the three values of Re .

2.3.3. Simplification of analytically determined velocity expressions

Equations (19) and (24)—for the preferred $n = 1$ case—are readily simplified in different limits of interest. It is simply shown by retaining leading terms that Eq. (19) for V_{pg} results in two separate regimes: $V_{pg} \propto St_L^{1/2}$ for $Re^{-1/2} < St_L \ll 1$ and $V_{pg} \propto St_L Re^{1/4}$ for $St_L < Re^{-1/2}$. This is confirmed by inspection of Figs. 2 and 4. While Eq. (19) is not formally valid for $St_L > 1$, inspection reveals that it does reach the correct limiting value. In the special case of

$St_\eta = 1$, or $St_L = Re^{-1/2}$, Eq. (19) reduces directly to

$$V_{pg}(St_\eta = 1) = V_g \frac{Re^{-1/4}}{\sqrt{2}} = c\alpha^{1/4} \left(\frac{v}{4cH} \right)^{1/4}, \quad (25)$$

where we have substituted $V_g = c\alpha^{1/2}$ (Cuzzi et al., 2001). This Re dependence, which also applies for $St_\eta < 1$ in general, quite naturally explains a result we obtained empirically from our numerical models over a range of Re much smaller than nebula values, namely that $V_{pg}/V_g \propto Re^{-1/4}$ (Cuzzi et al., 1998). By contrast, it is similarly shown from Eq. (20)

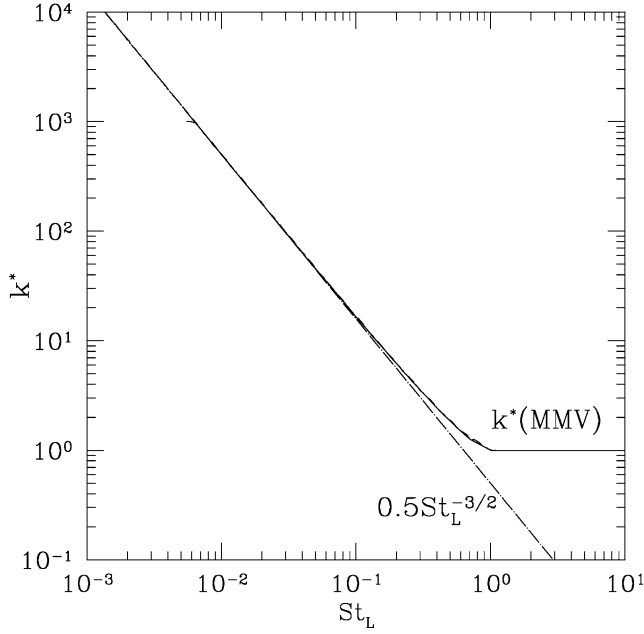


Fig. 3. Correction of our approximation $k^* \approx St_L^{-3/2}$ by a factor of 2 (dash-dot line), which brings it into excellent agreement (in our range of validity $St_L < 0.1$) with the exact numerical solution for k^* , shown with essentially overlapping curves for $Re = 10^4$, 10^7 , and 10^9 , computed using the full VJMR/MMV expression (solid line). Very close to $St_\eta = 1$ our approximation deviates slightly; notice the tiny tail at $St_L = 6 \times 10^{-3}$, $k^* = 10^3$, which is the Kolmogorov scale for $Re = 10^4$. The corresponding features for higher Re are off the plot to the left.

that the St_L dependence of V_{pg} for the older $n = 0$ case continues the $St_L^{1/2}$ dependence to arbitrarily small St_L .

These results are also consistent with arguments in Cuzzi et al. (1993, Appendix B; A. Dobrovolskis, personal communication). We can expand and time-average the instantaneous quantity $\langle (V_p - V_g)^2 \rangle$ to obtain $\langle V_{pg} V_{pg} \rangle = \langle V_p V_p \rangle + \langle V_g V_g \rangle - 2\langle V_p V_g \rangle$. Substituting from Cuzzi et al. (1993, Eq. (B11)) we find $\langle V_p V_p \rangle = \langle V_p V_g \rangle = \langle V_g V_g \rangle / (1 + St_L)$, leading to $V_{pg} = (St_L / (1 + St_L))^{1/2} V_g$, which reaches the same limits as Eq. (19) *except* for particles with $t_s \leq t_\eta$, or $St_\eta \leq 1$, because the integral in its derivation (Cuzzi et al., 1993, Eq. (B11)) extends to infinite eddy frequency.

Thus, unless $t_s \leq t_\eta$ ($St_L < Re^{-1/2}$), the particle-gas relative velocity in turbulence is generally proportional to $\sqrt{St_L}$ for small St_L . The steeper dependence of V_{pg} on St_L and St_η is restricted (in turbulence) to particles with $St_\eta \leq 1$. That is, evidence for a more nearly linear dependence of V_{pg} on r , if the environment was turbulent, would imply that the particles in question were $St_\eta \leq 1$ particles. This new result derives directly from the use of the $n = 1$ gas velocity autocorrelation function. The primary qualitative change is in the particle size dependence of V_{pg} for particles with $St_\eta \leq 1$. We address the significance of this in more detail in a forthcoming paper (Cuzzi, in preparation).

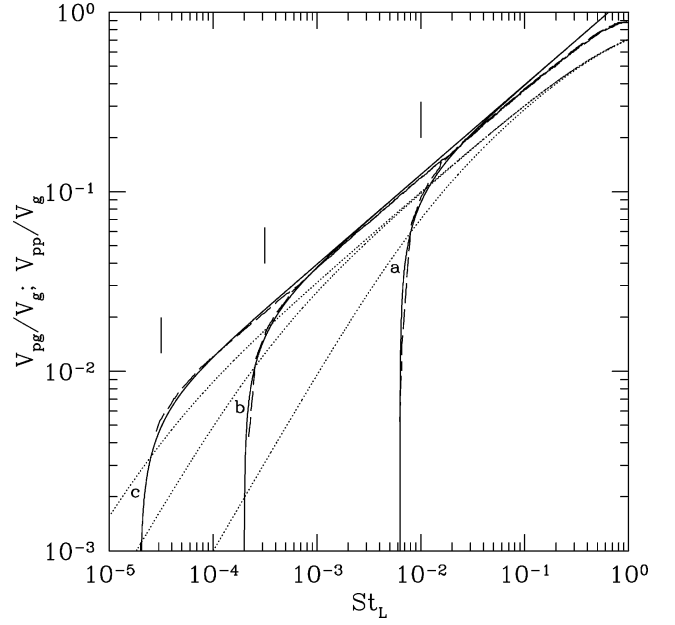


Fig. 4. $V_{pg}(St_L)$ (dotted; Eq. (19)), and $V_{pp}(St_L)$ (solid; Eq. (23)), for Re values of (a) 10^4 , (b) 10^7 , and (c) 10^9 . The digitized results of MMV (their Fig. 5) for V_{pp} , for the same three values of Re , are shown by the dashed lines. Our V_{pp} expression is invalid for $St_L > 0.1$ or so (see text).

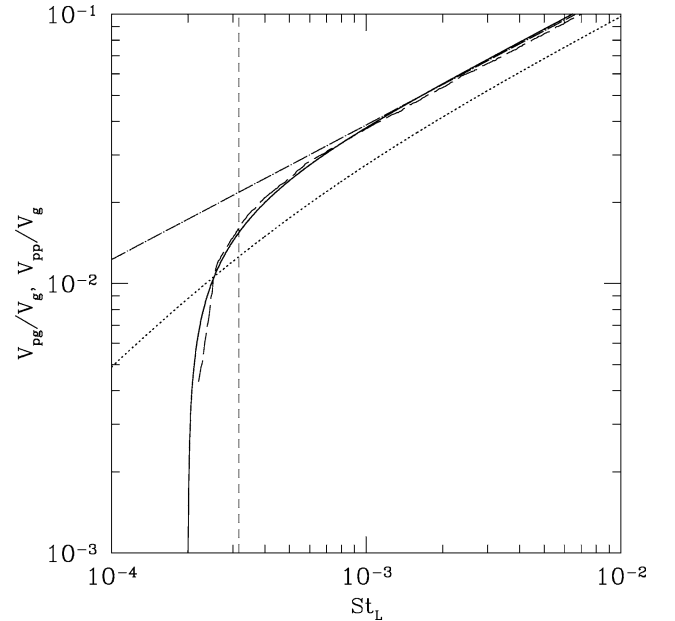


Fig. 5. A close-up plot of V_{pg} (dotted), V_{pp} (solid), and the digitized MMV results for V_{pp} (dashed; their Fig. 5), all for the $Re = 10^7$ case. The dash-dot line has slope $1/2$. The vertical short dashed line indicates $St_\eta = 1$, where $St_L = Re^{-1/2}$; here, $V_{pg} \propto St_L^{0.75}$.

Finally, using Eq. (24) for V_{pp} , we get

$$V_{pp}(St_\eta = 1) = \sqrt{0.8} V_g Re^{-1/4} = 1.26 V_{pg}, \quad (26)$$

where we used Eq. (25) for V_{pg} .

3. Comparison with numerical results

In this section we compare numerical results from our full 3D Lagrangian particle–gas model (Hogan et al., 1999) with full numerical calculations using our implementation of MMV (Section 2.3). We present particle velocities relative to the computational box (V_p) and relative to the local fluid velocity (V_{pg}), as obtained from our simulations. These velocities are defined as RMS spatial averages over all particles in a single snapshot, or $V = (\langle (V_x - \langle V_x \rangle)^2 \rangle + \langle (V_y - \langle V_y \rangle)^2 \rangle + \langle (V_z - \langle V_z \rangle)^2 \rangle)^{1/2}$, where V represents V_p or V_{pg} at the location of each particle, and $\langle \cdot \rangle$ is the averaging operator $\langle \cdot \rangle = \sum_{i=1}^{N_p} (\cdot) / N_p$, where N_p is the number of particles in a single snapshot. Of course, $\langle V \rangle$ is very close to zero for both these quantities since there is no mean flow in our simulations.

This spatial averaging approach is equivalent to the temporal averaging implicit in the MMV model, because of the ergodic principle that equates temporal and spatial averaging under suitable conditions. In our case, the conditions are satisfied because our integral length scale L is small compared to the spatial period of the computational domain, for all Re .

The case of V_{pp} is more complicated, as the results depend on the proximity region chosen for “neighboring” particles. For the most useful comparisons with the predictions of MMV and VJMR, and with the expected uses of this quantity in mind, the region over which particle neighbors are selected should be as small as possible—less than η certainly—and here we run into sampling errors. Perhaps most important, the deviation of our 3D model energy spectrum from a Kolmogorov spectrum is significant (e.g., Squires and Eaton, 1990), and V_{pp} is much more sensitive to the details of the high-spatial-frequency end of the energy spectrum than either V_p or V_{pg} . Since the main purpose of these calculations is to verify numerically the preference for the $n = 1$ autocorrelation function in an independent way from the direct comparison shown in Fig. 1, and because this case is already well made by the V_p and V_{pg} plots, we present no comparisons for V_{pp} .

Figures 6 and 7 show that the $n = 1$ autocorrelation function provides a much better fit to both V_p and V_{pg} than the $n = 0$ version. For V_{pg} , the fits of the MMV theory to our simulations are less perfect than for V_p . We can see several possible explanations for this. For instance, the mathematically simple form adopted for the $n = 1$ autocorrelation function is not a perfect fit to the actual numerically determined one (Fig. 1), by about the correct fractional amount. Also, we have emphasized that the correct velocity autocorrelation function to use is that *along a particle trajectory* (Meek and Jones, 1973), and this function is actually somewhat size dependent even over the range $St_\eta \sim 1$ (see, e.g., Squires, 1990, Fig. 4-23). Finally, because of the deviation of our turbulent kinetic energy spectrum from an inertial range, some of the definitions of eddy times used in the MMV theory might be inappropriate. It would not be surprising for

V_{pg} to be more sensitive to these small deviations than V_p (compare Figs. 6 and 7). In spite of the small deviations in V_{pg} , the combination of the direct comparisons of the

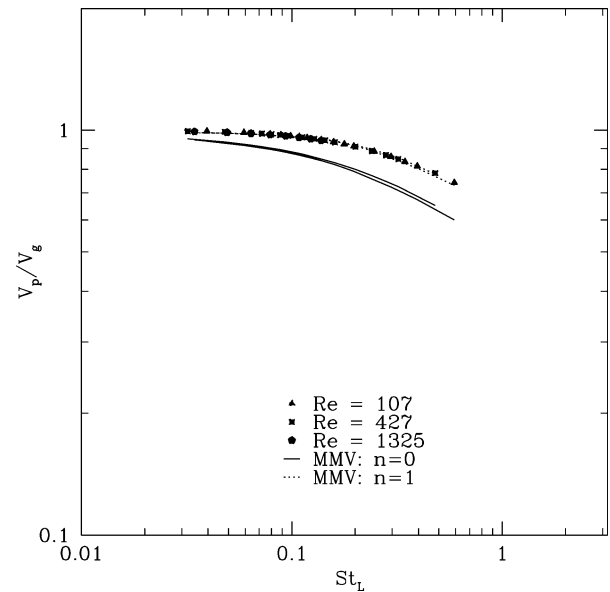


Fig. 6. V_p vs St_L obtained from our direct simulations (symbols) compared with MMV predictions for models $n = 0$ (solid line) and $n = 1$ (dotted line). All velocities have been normalized by the RMS fluid velocity V_g . Results are essentially Re independent. The St_L values for each point are defined relative to a large eddy time based on a *constant* large eddy time t_L , which is essentially the correlation time of Fig. 1. The $n = 1$ MMV prediction is clearly a better fit to the numerically simulated velocities.

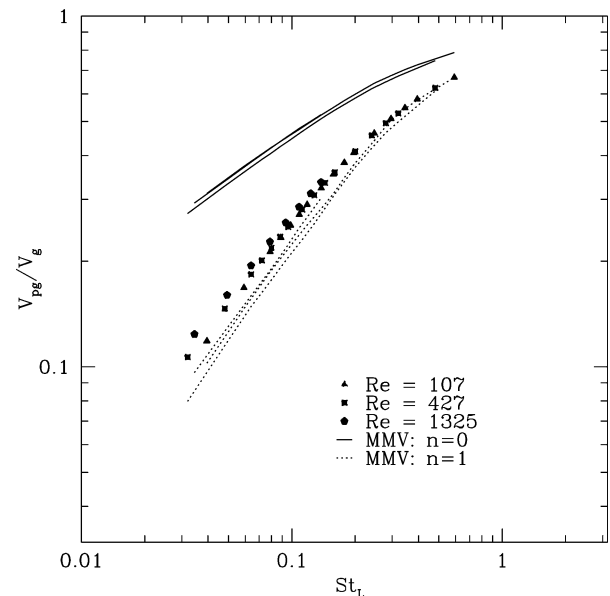


Fig. 7. V_{pg} obtained from our direct simulations (symbols), compared with predictions of the MMV models with $n = 0$ (solid lines) and $n = 1$ (dotted lines) vs St_L . All curves have been normalized by the RMS fluid velocity V_g . Here there is a small Re dependence, as seen in Fig. 2, for both the numerical calculations and theoretical predictions. The small deviation between the $n = 1$ calculations and the MMV theory is discussed in Section 3, but here again, $n = 1$ is much better than $n = 0$.

autocorrelation functions themselves (Fig. 1) and the comparison of the velocities derived using them (Figs. 6 and 7) makes it clear that the $n = 1$ autocorrelation function is the best choice.

4. Summary and conclusions

We have presented theoretical and numerical results which describe the turbulence-driven velocities of particles in the $St_L < 1$ size regime which might characterize chondrules and similar sized particles. The problem is fundamentally nonlinear because the perturbations on a particle depend on its trajectory, which is in turn determined by its perturbed velocity. Overall, we numerically verify, using full 3D turbulent calculations with particles, the general solution approach of Völk et al. (1980) as modified by Markiewicz et al. (1991). That is to say, we validate their approach to circumventing the “essential nonlinearity” of the problem (cf. Meek and Jones, 1973).

More specifically, we verify in two different ways the intuitive preference of MMV for a gas velocity autocorrelation function—at least along the trajectories of $St_L \ll 1$ particles. The MMV $n = 1$ velocity autocorrelation function leads to a particle–gas relative velocity function that approaches linear dependence on particle size for particles in the $St_\eta \approx 1$ regime and becomes and remains linear for arbitrarily small sizes. This is quite a different result than predicted by the original VJMR ($n = 0$) expressions.

Finally, we derive simple, closed-form, analytic expressions for V_p , V_{pg} , and V_{pp} (the latter, for comparable size particles only) for arbitrary levels of nebula intensity, as characterized by the flow Reynolds number Re or its corresponding “ α .” One immediate result of interest is that the velocity of small particles relative to a turbulent gas is approximately linearly dependent on particle stopping time, itself linearly proportional to particle radius in this regime. These expressions may be of broader general use.

Acknowledgments

We are grateful to Sandy Davis for helpful discussions on matters mathematical, to Robert Last for computational and graphics support, and to Wojtek Markiewicz for helpful discussions concerning MMV. We thank Ignacio Mosqueira, Steve Desch, Pat Cassen, Tony Dobrovolskis, and an anonymous reviewer for careful reading of the manuscript and helpful comments. This research was supported by grants to JNC from the Planetary Geology and Geophysics Program and the Origins of Solar Systems Program.

References

Adachi, I., Hayashi, C., Nakazawa, K., 1976. The gas drag effect on the elliptical motion of a solid body in the primordial solar nebula. *Prog. Theor. Phys.* 56, 1756–1771.

- Batchelor, G.K., 1948. Diffusion in a field of homogeneous turbulence II; the relative motion of particles. *Proc. Cambridge Philos. Soc.* 48, 345–362.
- Boss, A.P., 1996. A concise guide to chondrule formation models. In: Hewins, R., Jones, R., Scott, E.R.D. (Eds.), *Chondrules and the Protoplanetary Disk*. Cambridge Univ. Press, Cambridge, UK, pp. 257–264.
- Brearley, A.J., Jones, R.H., 1998. Chondritic meteorites. Chapter 3. In: *Planetary Materials*. In: *Reviews in Mineralogy*, Vol. 36, p. 191.
- Connolly, H.C., Love, S.G., 1998. The formation of chondrules: petrologic tests of the shock wave model. *Science* 280, 62–67.
- Csanady, G.T., 1963. Turbulent diffusion of heavy particles in the atmosphere. *J. Atmos. Sci.* 14, 171–194.
- Cuzzi, J.N., Davis, S.S., Dobrovolskis, A.R., 2003. Blowing in the wind: II. Creation and redistribution of refractory inclusions in a turbulent protoplanetary nebula. In: *Lunar Planet. Sci. Conf.*, pp. 34–35.
- Cuzzi, J.N., Dobrovolskis, A.R., Champney, J.M., 1993. Particle-gas dynamics near the midplane of a protoplanetary nebula. *Icarus* 106, 102–134.
- Cuzzi, J.N., Dobrovolskis, A.R., Hogan, R.C., 1996. Turbulence, chondrules, and planetesimals. In: Hewins, R., Jones, R., Scott, E.R.D. (Eds.), *Chondrules and the Protoplanetary Disk*. Cambridge Univ. Press, Cambridge, UK, pp. 35–44.
- Cuzzi, J.N., Hogan, R.C., Paque, J.M., Dobrovolskis, A.R., 1998. Chondrule rimming by sweepup of dust in the protoplanetary nebula: constraints on primary accretion. In: *Lunar Planet. Sci. Conf.*, p. 29.
- Cuzzi, J.N., Hogan, R.C., Paque, J.M., Dobrovolskis, A.R., 2001. Size-selective concentration of chondrules and other small particles in protoplanetary nebula turbulence. *Astrophys. J.* 546, 496–508.
- Dubrulle, B., Morfill, G.E., Sterzik, M., 1995. The dust sub-disk in the protoplanetary nebula. *Icarus* 114, 237–246.
- Elghobashi, S.E., 1991. Particle-laden turbulent flows: direct simulation and closure models. *Appl. Sci. Res.* 48, 301–314.
- Grossman, J., 1989. Formation of chondrules. In: Kerridge, J.F., Matthews, M.S. (Eds.), *Meteorites and the Early Solar System*. Univ. of Arizona Press, Tucson, pp. 680–696.
- Grossman, J., Rubin, A.E., Nagahara, H., King, E.A., 1989. Properties of chondrules. In: Kerridge, J.F., Matthews, M.S. (Eds.), *Meteorites and the Early Solar System*. Univ. of Arizona Press, Tucson, pp. 619–659.
- Hinze, J.O., 1975. *Turbulence*, 2nd edition. McGraw–Hill, New York.
- Hogan, R.C., Cuzzi, J.N., Dobrovolskis, A.R., 1999. Scaling properties of particle density fields formed in turbulent flows. *Phys. Rev. E* 60, 1674–1680.
- Jones, R.H., Lee, T., Connolly Jr., H.C., Love, S.G., Shang, H., 2000. Formation of chondrules and CAIs: theory vs. observation. In: Mannings, V., Boss, A.P., Russell, S.S. (Eds.), *Protostars and Planets IV*. Univ. of Arizona Press, Tucson, p. 927.
- Markiewicz, W.J., Mizuno, H., Völk, H.-J., 1991. Turbulence-induced relative velocity between two grains. *Astron. Astrophys.* 242, 286–289.
- Meek, C.C., Jones, B.G., 1973. Studies of the behavior of heavy particles in a turbulent fluid flow. *J. Atmos. Sci.* 30, 239–244.
- Metzler, K., Bischoff, A., 1996. Constraints on chondrite agglomeration from fine-grained chondrule rims. In: Hewins, R., Jones, R., Scott, E.R.D. (Eds.), *Chondrules and the Protoplanetary Disk*. Cambridge Univ. Press, Cambridge, UK.
- Morfill, G.E., Durisen, R.H., Turner, G.W., 1998. Note: An accretion rim constraint on chondrule formation theories. *Icarus* 134, 180–184.
- Nakao, H., 1997. Exact expression of Lagrangian velocity autocorrelation function in isotropic homogeneous turbulence. *Monte Carlo Meth. Appl.* 3, 225–240.
- Paque, J., Cuzzi, J.N., 1997. Physical characteristics of chondrules and rims, and aerodynamic sorting in the solar nebula. In: *Lunar Planet. Sci. Conf.*, p. 28.
- Squires, K., 1990. *The Interaction of Particles with Homogeneous Turbulence*. Thesis. Stanford University.
- Squires, K., Eaton, J.K., 1990. Particle response and turbulence modification in isotropic turbulence. *Phys. Fluids A* 2, 1191–1203.

- Squires, K., Eaton, J.K., 1991. Lagrangian and Eulerian statistics obtained from direct numerical simulations of homogeneous turbulence. *Phys. Fluids A* 3, 1169–1178.
- Tennekes, H., Lumley, J.L., 1972. *A First Course in Turbulence*. MIT Press, Cambridge, MA.
- Vincent, A., Meneguzzi, M., 1991. The spatial structure and statistical properties of homogeneous turbulence. *J. Fluid Mech.* 225, 1–20.
- Völk, H.J., Jones, F.C., Morfill, G.E., Röser, S., 1978. Induced velocities of grains embedded in a turbulent gas. *Moon Planets* 19, 221–227.
- Völk, H.J., Jones, F.C., Morfill, G.E., Röser, S., 1980. Collisions between grains in a turbulent gas. *Astron. Astrophys.* 85, 316–325.
- Weidenschilling, S.J., 1977. Aerodynamics of solid bodies in the solar nebula. *Mon. Not. R. Astron. Soc.* 180, 57–70.
- Weidenschilling, S.J., 1980. Dust to planetesimals: settling and coagulation in the solar nebula. *Icarus* 44, 172–189.
- Whipple, F., 1973. Radial pressure in the solar nebula as affecting the motions of planetesimals. In: Hemenway, C.L., Millman, P.M., Cook, A.F. (Eds.), *Evolutionary and Physical Properties of Meteoroids*. In: *Proc. IAU Colloq.*, Vol. 13, p. 355, NASA SP 319.